

Quasi-Linear Optical Pulses in Dispersion Managed Fibers: Propagation and Interaction

Mark J. Ablowitz and Toshihiko Hirooka

Department of Applied Mathematics, University of Colorado at Boulder
Boulder, CO 80309-0526, USA

1 Introduction

In recent years, considerable research has been devoted to the study of fiber-optic communication systems employing dispersion management for both soliton and non-soliton transmission. In a dispersion-managed system, the fiber is made up of alternating sections of positive and negative group-velocity dispersion (GVD) in such a manner as to create a transmission line with high local and low average dispersion.

In soliton transmission, dispersion management was first introduced to overcome the Gordon-Haus jitter, i.e., timing jitter of solitons arising from their interaction with amplifier noise [1], without degrading the signal-to-noise ratio (SNR) [2]. The motivation was to reduce the Gordon-Haus effect by compensating for dispersion accumulation periodically, since Gordon-Haus jitter is proportional to the accumulated dispersion. Later it was shown numerically that there exists a nonlinear localized solution in a dispersion-managed system, now referred to as a dispersion-managed (DM) soliton, which propagates with periodically changing its shape [3]. The DM soliton is found to have enhanced energy compared to the energy of the soliton in a fiber with constant dispersion equal to the average dispersion. This allows one to reduce the Gordon-Haus effect by lowering the average dispersion without sacrificing the degradation of SNR.

In non-soliton transmission, dispersion management is found to manage fiber nonlinearity and suppress certain nonlinear effects such as self-phase modulation [4,5] and inter-channel crosstalk in wavelength division multiplexed (WDM) systems [6–9]. In a strongly dispersion-managed transmission line, because of high local dispersion, the pulse width expands considerably and thus the peak power is suppressed locally, which in turn mitigates the nonlinearity. Such a system is hence commonly referred to as quasi-linear. In contrast to DM solitons, in quasi-linear system the effective nonlinearity is mitigated for large map strength, and the spectral intensity is found to be an invariant of the propagation in the lossless case [4].

We note the difference between DM soliton transmission where nonlinearity balances dispersion, as compared to quasi-linear transmission in which nonlinearity is managed. Nevertheless, independent of transmission format, the pulse dynamics in dispersion-managed optical fibers is described by the perturbed nonlinear Schrödinger (NLS) equation, where the dispersion coefficient is now varying rapidly as a periodic function of distance. By introducing multiple scales

and separating fast scale dynamics due to the large and periodic perturbation from the perturbed NLS equation, one obtains an averaged evolution equation which governs the pulse dynamics over a slow scale characterized by the nonlinear length [10]. The obtained model, referred to as the dispersion-managed NLS (DMNLS) equation, elucidates the role of nonlinearity in dispersion-managed transmission independent of transmission format, and thus provides a unified analytical description of DM soliton and quasi-linear transmission.

Dispersion management considerably modifies the dynamics of pulse evolution because of the periodic variation of GVD. The alternating GVD sign within one period brings about large pulse width oscillation. This leads to strong overlap of neighboring bits in a pulse train, resulting in significant nonlinear interactions [11,12]. Dispersion management also alters the sign of the velocity of the pulse within each map period, and thus the trajectory of the central pulse position draws large zigzags. This zigzag motion leads to repeated collisions among pulses in different wavelength channels in WDM transmission [13,14].

In DM soliton transmission, WDM interactions due to the repeated collisions is found to be a major transmission penalty [15,16]. They are responsible for timing jitter and may even result in collapse. On the other hand, in quasi-linear transmission, because of their strong overlap, residual nonlinearity induces intra-channel crosstalk between adjacent pulses, which lead to serious transmission penalties such as timing and amplitude jitter of the main signals (the 1's) [17–20] and ghost pulse generation at 0 bits [21].

In this article, we present an analytical framework that describes the propagation and interaction of quasi-linear optical pulses in strongly dispersion-managed transmission systems. Preliminary remarks on the normalizations and units of the perturbed NLS equation are summarized in Section 2. We introduce multiple scale analysis and derive the DMNLS equation from the perturbed NLS equation in Section 3. In Section 4 we investigate the pulse evolution and elucidate the role of nonlinearity in quasi-linear transmission using the DMNLS equation. In Section 5, we develop an analytical model to study intra-channel pulse interactions in quasi-linear transmission based on the DMNLS equation.

2 Perturbed nonlinear Schrödinger equation

Propagation of optical pulses in dispersion-managed fibers in the presence of loss and amplification is described by the perturbed NLS equation

$$i \frac{\partial u}{\partial z} + \frac{D(z)}{2} \frac{\partial^2 u}{\partial t^2} + g(z) |u|^2 u = 0, \quad (1)$$

where all the quantities are expressed in dimensionless units: $t = t_{\text{ret}}/t_*$, $z = z_{\text{lab}}/z_*$, $u = E/\sqrt{gP_*}$, $D = k''/k_*''$ with the characteristic parameters denoted by the subscript *, where t_{ret} and z_{lab} are the retarded time and the propagation distance, respectively, and E denotes the slowly varying envelope of the optical field. The normalizing variables are determined so that $z_* = z_{\text{NL}} \equiv 1/\nu P_*$ and $k_*'' = -t_*^2/z_{\text{NL}}$ where ν is the nonlinear coefficient. The functions $D(z)$ and $g(z)$

describe the local GVD of the fiber and the variation of power due to loss and amplification, respectively, which are both periodic in z with period z_a . The nonlinear coefficient $g(z)$ for lumped amplification based on EDFA's is given by

$$g(z) = g_e \exp[-2\Gamma(z - nz_a)], \quad nz_a \leq z < (n+1)z_a, \quad (2)$$

where $g_e = 4G/[1 - \exp(-4G)]$ so that $\langle g \rangle = 1$ ($\langle \cdot \rangle$ denotes the path-average over z_a), Γ is the dimensionless loss coefficient, and $G = \Gamma z_a/2$. We write the accumulated dispersion in the form

$$\bar{D}(z) = \int_0^z D(z') dz' = C(z) + \langle D \rangle z, \quad (3)$$

where $\langle D \rangle$ is the average dispersion over a period and $C(z)$ is a periodic function with period z_a having zero average $\langle C \rangle = 0$.

3 Dispersion managed nonlinear Schrödinger equation

In order to model strong dispersion management, we decompose the GVD $D(z)$ into two parts: a path-average constant $\langle D \rangle$ and the rapidly varying function Δ corresponding to local GVD:

$$D(z) = \langle D \rangle + \frac{1}{z_a} \Delta(z/z_a), \quad (4)$$

where $z_a (\ll 1)$ is the map period. Note that Δ/z_a represents a large variation about the average due to strong dispersion management and thus the proportionality factor $1/z_a$ is required in front of $\Delta(z/z_a)$ so that both $\langle D \rangle$ and Δ are quantities of order one. Since the perturbed NLS equation with $D(z)$ given by (4) contains both slowly and rapidly varying terms, it is convenient to introduce the fast and slow scales as $\zeta = z/z_a$ and z respectively. We also expand the field u in powers of z_a :

$$u(\zeta, z, t) = u^{(0)}(\zeta, z, t) + z_a u^{(1)}(\zeta, z, t) + \dots \quad (5)$$

The perturbed NLS equation is now broken into a series of equations corresponding to the different powers of z_a . At the leading order in the expansion $O(1/z_a)$, we have

$$i \frac{\partial u^{(0)}}{\partial \zeta} + \frac{\Delta(\zeta)}{2} \frac{\partial^2 u^{(0)}}{\partial t^2} = 0, \quad (6)$$

namely the evolution of the pulse is determined solely by the large variations of $D(z)$ about the average, and nonlinearity and residual dispersion represent only a small perturbation to the linear solution. Eq. (6) can be solved by the Fourier transform

$$\hat{u}^{(0)}(\zeta, z, \omega) = \mathcal{F} \left[u^{(0)} \right] = \int_{-\infty}^{\infty} u^{(0)}(\zeta, z, t) \exp(-i\omega t) dt,$$

and the solution is given by

$$\hat{u}^{(0)}(\zeta, z, \omega) = \hat{U}(z, \omega) \exp[-iC(\zeta)\omega^2/2], \quad C(\zeta) = \int_0^\zeta \Delta(\zeta')d\zeta', \quad (7)$$

where $\hat{U}(z, \omega)$ is the integration constant in terms of ζ and represents the slowly evolving amplitude of $\hat{u}^{(0)}$, whose exact form is determined from the higher order in the expansion.

At the next order in the expansion $O(1)$, we have (in the frequency domain)

$$i\frac{\partial \hat{u}^{(1)}}{\partial \zeta} - \frac{\langle D \rangle}{2}\omega^2 \hat{u}^{(1)} = -\hat{P}^{(1)}, \quad \hat{P}^{(1)} = i\frac{\partial \hat{u}^{(0)}}{\partial z} - \frac{\langle D \rangle}{2}\omega^2 \hat{u}^{(0)} + g(z)\mathcal{F} \left[|u^{(0)}|^2 u^{(0)} \right], \quad (8)$$

which is written in a more convenient form as

$$i\frac{\partial}{\partial \zeta} \left[\hat{u}^{(1)} \exp(iC\omega^2/2) \right] = -\hat{P}^{(1)} \exp(iC\omega^2/2). \quad (9)$$

In order to remove secularities, namely to avoid resonant growth of $u^{(1)}$ so that the expansion of u in powers of z_a in (5) is remained to be well ordered, we require the following condition:

$$\int_0^1 \hat{P}^{(1)} \exp(iC\omega^2/2) d\zeta = 0. \quad (10)$$

This condition yields the following equation for \hat{U} :

$$i\frac{\partial \hat{U}}{\partial z} - \frac{\langle D \rangle}{2}\omega^2 \hat{U} + \int_{-\infty}^{\infty} \int_{-\infty}^{\infty} r(\omega_1 \omega_2) \hat{U}(z, \omega + \omega_1) \hat{U}(z, \omega + \omega_2) \times \hat{U}^*(z, \omega + \omega_1 + \omega_2) d\omega_1 d\omega_2 = 0, \quad (11)$$

where the kernel

$$r(x) = \frac{1}{(2\pi)^2} \int_0^1 g(\zeta) \exp(iC(\zeta)x) d\zeta \quad (12)$$

represents the structure of GVD profile.

Let us consider two special cases. First, when there is no loss and amplification ($g(z) = 1$), the kernel $r(x)$ of a piecewise constant dispersion map (see Fig. 1) is given by $r(x) = (1/(2\pi)^2) \sin sx/sx$, where $s = [\theta\Delta_1 - (1-\theta)\Delta_2]/4$ is a measure of dispersion map strength. Secondly, if the dispersion has no periodic variations ($\Delta = 0$ and thus $s = 0$), then $r(x) = 1/(2\pi)^2$ and the DMNLS equation reduces to the standard NLS equation, i.e., Eq. (1) with $D(z) = g(z) = 1$.

Special stationary solutions of the DMNLS equation are obtained by looking for solutions of the form $\hat{U}(z, \omega) = F(\omega) \exp(i\lambda^2 z/2)$ which yields the following nonlinear integral equation for $F(\omega)$:

$$(\lambda^2 + \langle D \rangle \omega^2) F(\omega) = 2 \int_{-\infty}^{\infty} \int_{-\infty}^{\infty} r(\omega_1 \omega_2) F(\omega + \omega_1) F(\omega + \omega_2) F^*(\omega + \omega_1 + \omega_2) d\omega_1 d\omega_2. \quad (13)$$

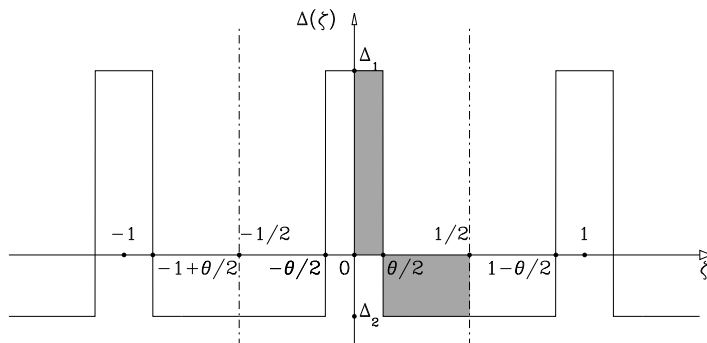


Fig. 1. Schematic diagram of a two-step dispersion map.

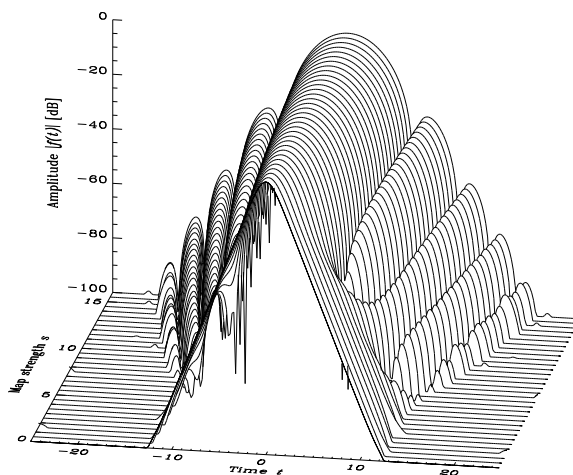


Fig. 2. The shape of the stationary pulses for $\langle D \rangle = 1$, $\lambda = 1$ and various values of s .

A rapidly convergent procedure to solve this numerically is described in [22]. The obtained solution is the stationary DM soliton pulses. Some typical pulses are depicted in Fig. 2. We note that (13) contains a parameter λ which characterizes the mode, corresponding to the energy. The main features of the DM solitons for large s are a Gaussian like center with exponentially decaying and oscillating tails. For small s , the mode approaches the classical soliton profile.

The fast scale evolution (i.e., with respect to ζ) can be reconstructed by multiplying $\exp(-iC\omega^2/2)$ with the slowly varying Fourier amplitude \hat{U} . When observed in this scale the pulse shape is changing periodically because of the

local GVD variation, whereas the pulse propagates without changing its shape on a slow scale which is characterized by nonlinearity and the average dispersion. Thus DM soliton is considered to be a stationary pulse where nonlinearity balances the average dispersion.

4 Quasi-linear pulse propagation

The evolution of pulses in the quasi-linear regime ($s \gg 1$) can also be studied based on the DMNLS equation [4,5]. To analyze the behavior of quasi-linear pulses, we assume that $\hat{U}(z, \omega)$ depends only weakly on s and compute an asymptotic expansion of the nonlinear nonlocal term in (11) for $s \gg 1$.

4.1 Lossless case

When $g(z) = 1$ (i.e., in a lossless system), we have

$$i \frac{\partial \hat{U}}{\partial z} - \frac{\langle D \rangle}{2} \omega^2 \hat{U} + \Psi [|\hat{U}|^2] \hat{U} = 0, \quad (14)$$

$$\Psi [|\hat{U}(z, \omega)|^2] = \frac{1}{2\pi s} \left[(\log s - \gamma) |\hat{U}(z, \omega)|^2 - \int_{-\infty}^{\infty} H(\omega' - \omega) |\hat{U}(z, \omega')|^2 d\omega' \right], \quad (15)$$

where $\gamma = 0.57722$ is Euler's constant and $H(\omega) = (1/\pi) \int_{-\infty}^{\infty} \log |t| \exp(-i\omega t) dt$. Eq. (14) can be solved explicitly as

$$\hat{U}(z, \omega) = \hat{U}(0, \omega) \exp \left\{ -i \langle D \rangle \omega^2 z / 2 + i \Psi [|\hat{U}(0, \omega)|^2] z \right\}. \quad (16)$$

From these results, we note the following important observations in terms of pulse dynamics in the quasi-linear regime. First, nonlinearity is mitigated by $O(\log s/s)$ and vanishes in the limit $s \rightarrow \infty$. In other words, the quasi-linear system is in the regime where nonlinearity is managed. Secondly, nonlinearity is responsible only for phase shift $\phi_{\text{NL}}(z, \omega) = \Psi[|\hat{U}(0, \omega)|^2]z$ in frequency domain, and thus the spectral intensity $|\hat{U}(z, \omega)|$ is preserved during propagation, as opposed to the self-phase modulation in standard fibers. Finally we also note that the quasi-linear pulse can be viewed as degenerate limit of a DM soliton. The DM soliton satisfies the DMNLS equation with $\hat{U}(z, \omega) = F(\omega) \exp(i\lambda^2 z/2)$, where $F(\omega)$ is the solution of (14) and can be approximated by a Gaussian $F(\omega) \sim \alpha(\lambda) \exp(-\beta(\lambda)\omega^2/2)$. A quasi-linear Gaussian pulse has the same structure but is independent of the ‘‘eigenvalue’’ λ . The quasi-linear pulse can thus be looked at as a limit $\lambda \rightarrow 0$ in DM solitons. Importantly, both types of transmission format can be described with the same analytical framework.

To test our model, we compared the analytical results with direct numerical simulations of Eq. (1) with $\langle D \rangle = 0$ and $z_a = 0.1$. The incident pulse is given by a Gaussian $u(0, t) = (1/\sqrt{\beta}) \exp(-t^2/\beta)$. With the choice of $t_* = 2.2$ ps, $\nu = 2.2$ W⁻¹km⁻¹, and $P_* = 1$ mW (i.e. $z_{\text{NL}} = 450$ km and $k_*'' = -0.01$ ps²/km), $\beta = 1$

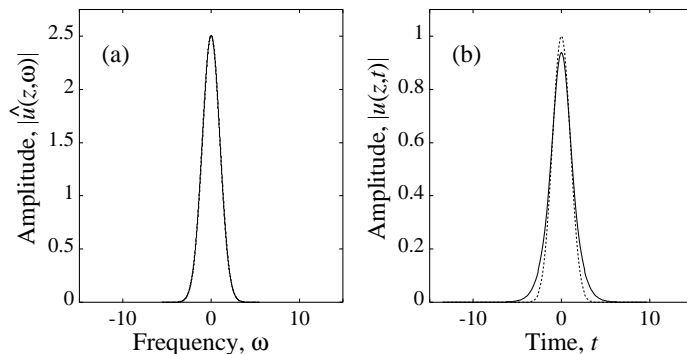


Fig. 3. Shape of the quasi-linear Gaussian pulse after a propagation of $z = 20$ (solid curves) and the initial profile (dotted curves) for $s = 100$, $\langle D \rangle = 0$, and $G = 0$: (a) frequency domain, (b) time domain. In (a), the dotted curve is indistinguishable from the solid curve.

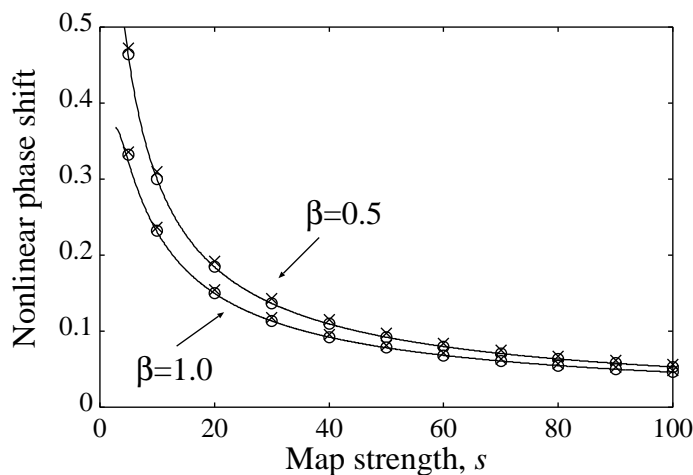


Fig. 4. Nonlinear phase shift $\phi_{\text{NL}}(\omega = 0)$ of the quasi-linear Gaussian pulse with $\beta = 0.5, 1$. The solid curve is the analytical result (see text), and the circles and crosses are the numerical results obtained from the direct simulation of Eq. (1) with $G = 0$ and $G = 0.5$, respectively.

corresponds to the peak power of 1 mW and FWHM of 3.7 ps (at minimum). The fiber loss is 0.2 dB/km and the amplifier period is 45 km. For this initial profile, the nonlinear phase shift at $\omega = 0$ is given by $\phi_{\text{NL}}(z, 0) = (1/s) \log(s/\beta)z$.

In Fig. 3, we plot the shape of the quasi-linear pulse when $s = 100$ after a propagation of $z = 20$ (9000 km), as well as the initial profile with $\beta = 1$. As predicted from the model, the spectral intensity is an invariant of the propagation, whereas small pulse broadening induced by the nonlinearity is observed in the time domain as a result of the acquired nonlinear chirp $\partial\phi_{\text{NL}}/\partial\omega$ in the

frequency domain (which is similar to the self-phase modulation in the time domain).

Figure 4 shows a plot of the phase shift $\phi_{\text{NL}}(z, \omega = 0)$ at $z = 1$ as a function of s for $\beta = 0.5$ and 1. The nonlinear phase shift is indeed decreasing for large s as $O(\log s/s)$, which further confirms the validity of the asymptotic expansion of Eq. (14) and (15). In this figure, we also plot $\phi_{\text{NL}}(\omega = 0)$ in the presence of loss ($G = 0.5$), which also follows similar lines as the lossless case. Detailed asymptotic analysis in the system with loss and amplification is presented in the next section.

4.2 Lossy case

When $g(z) \neq 1$ (i.e., in the presence of loss and amplification), the kernel $r(x)$ depends not only on s but also on the relative location of the amplifier within one dispersion map period, and the asymptotic analysis must be modified accordingly. In all cases, the nonlinearity is again mitigated by $O(\log s/s)$. However, the spectral characteristics of the pulse evolution depends strongly on the amplifier locations. We define ζ_a to represent the position of the amplifier within the dispersion map ($-1/2 \leq \zeta < 1/2$). For instance, $\zeta_a = 0$ means that the amplifier is located at the midpoint of the anomalous GVD segment, and $\zeta_a = 1/4$ corresponds to the boundary between normal and anomalous GVD segment (see also Fig. 1).

When the amplifiers are placed at the locations where the sign of GVD changes (i.e., $\zeta_a = \pm 1/4$), Eq. (11) is reduced to (14) but with

$$\Psi \left[|\hat{U}(z, \omega)|^2 \right] = \frac{1}{s} \left[(L_0 \log s - L_1) |\hat{U}(z, \omega)|^2 - L_0 \int_{-\infty}^{\infty} H(\omega' - \omega) |\hat{U}(z, \omega')|^2 d\omega' \right], \quad (17)$$

and the constants L_0 and L_1 defined as

$$L_0 = \frac{G}{2\pi} \exp(-2G) \text{csch} G, \quad (18a)$$

$$L_1 = \frac{G}{4\pi} \exp(-G) \text{csch} G [\exp(G) I_{G1} + \exp(-G)(3\gamma + \log G - I_{G2})] - \frac{G}{2\pi} \exp(G) I_{G1}, \quad (18b)$$

$I_{G1} = \int_G^\infty dx \exp(-x)/x$, and $I_{G2} = \int_0^G dx (\exp(x) - 1)/x$. Neglecting $O(1/s^2)$ terms, the spectral intensity $|\hat{U}(z, \omega)|^2$ is still preserved during pulse propagation, and the solution is (16) with $\Psi[|\hat{U}|^2]$ in (17). After the linear phase shift $\exp(-i(D)\omega^2 z/2)$ is removed by means of pre- or post-transmission compensation, the averaged dynamics of the quasi-linear pulse transmission is characterized only by the nonlinear phase shift $\phi_{\text{NL}}(z, \omega) = \Psi[|\hat{U}(0, \omega)|^2]z$ as in the lossless limit $G \rightarrow 0$ ($L_0 \rightarrow 1/2\pi$ and $L_1 \rightarrow \gamma/2\pi$).

When the amplifiers are placed in the middle of the normal or anomalous GVD segment ($\zeta_a = -1/4 \pm 1/4$, i.e., $\zeta_a = 0$ and $-1/2$), the spectral intensity

varies as $O(1/s)$ and spectral compression or broadening is observed respectively. In this case (30) is written as

$$i\frac{\partial\hat{U}}{\partial z} - \frac{\langle D \rangle}{2}\omega^2\hat{U} + \Psi[|\hat{U}|^2]\hat{U} \mp i\frac{K_2}{s}\hat{J}(z,\omega) = 0, \quad (19)$$

where $\Psi[|\hat{U}|^2]$ is now given by

$$\Psi[|\hat{U}(z,\omega)|^2] = \frac{1}{s} \left[(K_0 \log s - K_1)|\hat{U}(z,\omega)|^2 - K_0 \int_{-\infty}^{\infty} H(\omega' - \omega)|\hat{U}(z,\omega')|^2 d\omega' \right], \quad (20)$$

with the constants K_0 , K_1 , and K_2 defined as

$$K_0 = \frac{G}{2\pi}(\exp(-G)\operatorname{csch}G + 1), \quad (21a)$$

$$K_1 = \frac{G}{4\pi}\operatorname{csch}G[\exp(G)I_{G1} + \exp(-G)(3\gamma + \log G - I_{G2})] + \frac{G}{2\pi}(2\gamma + \log G), \quad (21b)$$

$$K_2 = \frac{G}{4}, \quad (21c)$$

and

$$\hat{J}(z,\omega) = \int_{-\infty}^{\infty} \int_{-\infty}^{\infty} \frac{d\omega_1 d\omega_2}{\omega_1 \omega_2} \hat{U}(z,\omega + \omega_1) \hat{U}(z,\omega + \omega_2) \hat{U}^*(z,\omega + \omega_1 + \omega_2). \quad (22)$$

In the limit of $G \rightarrow 0$, Eq. (19) reduces to Eq. (14) with (15) ($K_0 \rightarrow 1/2\pi$, $K_1 \rightarrow \gamma/2\pi$, and $K_2 \rightarrow 0$). From (19), the evolution of the intensity is described as

$$\frac{\partial|\hat{U}|^2}{\partial z} = \pm \frac{K_2}{s} f(z,\omega), \quad (23)$$

where $f(z,\omega) = \hat{J}(z,\omega)\hat{U}^*(z,\omega) + \hat{J}^*(z,\omega)\hat{U}(z,\omega)$. Since s is large, the solution of (23) can be approximated by

$$|\hat{U}(z,\omega)|^2 \approx |\hat{U}(0,\omega)|^2 \pm \frac{K_2 z}{s} f(0,\omega) \quad (24)$$

for moderate values of z .

In Fig. 5 we show a comparison of the spectral profile of a quasi-linear Gaussian pulse with $\beta = 1$ when $s = 50$, $\langle D \rangle = 0$, $z_a = 0.1$, and $G = 0.5$ (namely $\Gamma = 10$), after a propagation of $z = 20$ as well as the initial profile, with (a) $\zeta_a = 0$ (when amplifiers are located in the middle of anomalous GVD segments) and (b) $-1/2$ (in the middle of normal GVD segments). We see that the nonlinearity yields spectral compression and broadening when $\zeta_a = 0$ and $-1/2$ respectively. Remarkable agreement between the analysis and numerical results is obtained, which further confirms the validity of our model. Since the spectral evolution is a consequence of the nonlinearity, spectral reshaping may be observed by increasing the launch power. Note, however, that the nonlinearity is mitigated for large s , by $O(\log s/s)$ and the spectral reshaping effect is $O(1/s)$.

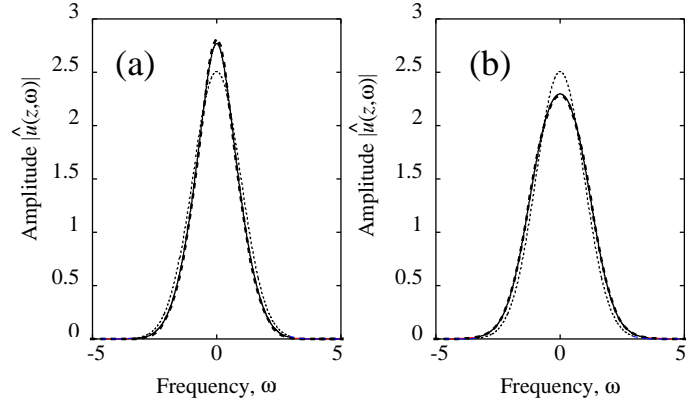


Fig. 5. The spectrum of the quasi-linear Gaussian pulse for $s = 50$: (a) $\zeta_a = 0$; (b) $\zeta_a = -1/2$. The solid curve is the pulse at $z = 20$ (i.e., $z_{\text{lab}} = 9000$ km) obtained from the direct simulation, and the dashed curve shows the analytical result. The dotted curve is the initial profile.

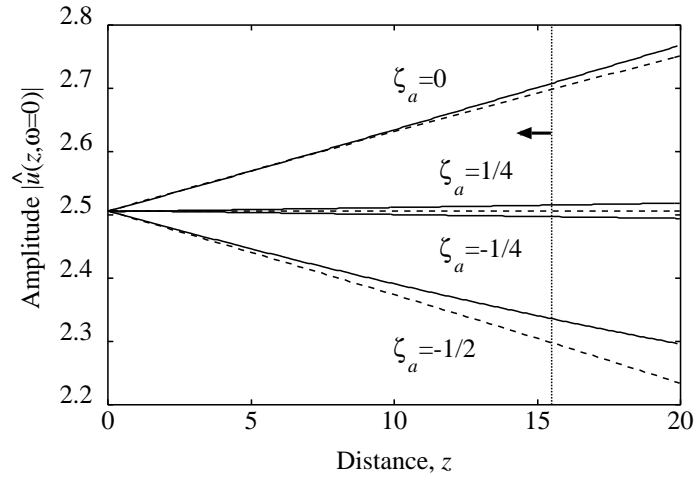


Fig. 6. The evolution of the spectral peak amplitude $|\hat{u}(z, \omega=0)|$ for several values of ζ_a . Solid lines are the results obtained from the direct simulation, and the dashed lines show the analytical approximation obtained from (24). Dotted line shows a reasonable upper limit of the validity of (24).

We also note that when $\zeta_a = 0$ or $-1/2$, since the spectral reshaping is not associated with phase modulation, the observed spectral compression/broadening accompanies pulse broadening/compression respectively in the time domain. This implies the possibility of transform-limited temporal or spectral compression of laser pulses. The analysis presented here is consistent with the recent

experimental and numerical observations of spectral compression of RZ pulses in strongly dispersion-managed lines [23–25].

Fig. 6 shows the evolution of the spectral peak amplitude $|\hat{u}(z, \omega = 0)|$ for $s = 50$, with $\zeta_a = 0, -1/2, -1/4$ (when amplifiers are positioned at the boundary between anomalous and normal GVD segments), and $1/4$ (at the boundary between normal and anomalous GVD segments), obtained from direct numerical simulation and the analytical approximation (24). Since energy is conserved during propagation, the increase and decrease of the peak amplitude when $\zeta_a = 0$ and $-1/2$ demonstrates the spectral compression and broadening respectively. On the other hand, with $\zeta_a = -1/4$ and $1/4$ the spectrum is still conserved, namely nonlinearity is responsible only for a phase shift. The deviation of the analytical approximation from the numerics for large z is a consequence of the growth of the term $(K_2 z/s)f(0, \omega)$ in (24). To be valid, $(K_2 z/s)f(0, \omega)/|\hat{U}(0, 0)|^2$ should be small. We also plot a reasonable upper limit for the validity of the asymptotics [namely $z < (K_2/s)f(0, \omega) = 15.5$ (7000 km)].

5 Intra-channel quasi-linear pulse interactions

We have seen in the previous section that nonlinearity is mitigated by the factor $O(\log s/s)$ in the quasi-linear regime. This suggests the employment of strong dispersion management with large map strength s .

As s increases, however, different forms of nonlinear interactions take place and result in the main source of signal deformation. In a strongly dispersion managed system, quasi-linear pulses in neighboring bit slots interact with each other because of their large overlap which is as a result of large pulse width broadening associated with high local GVD. This overlap induces nonlinear mixing (crosstalk) between pulses such as their frequency modulation and energy exchange, and leads to the fluctuation of the temporal position and amplitude of the pulses in “1” bits and the generation of “ghost” pulses in “0” bits [19–21]. The timing and amplitude jitter and the ghost pulse growth impose a major limitation to system performance in the quasi-linear regime with large s .

In order to study nonlinear intra-channel interactions between the main signal u_0 and the adjacent pulses u_l, u_m, u_n (u_k represents the signal pulse centered at $t = kT$, where T is the bit interval and k is the integer representing the location of the bit slot), we write $u = u_0 + u_l + u_m + u_n$ and substitute this into (1) to find the evolution of u_0 perturbed by one of the nonlinear terms $u_l^* u_m u_n$:

$$i \frac{\partial u_0}{\partial z} + \frac{D(z)}{2} \frac{\partial^2 u_0}{\partial t^2} + g(z) |u_0|^2 u_0 = -g(z) u_l^* u_m u_n. \quad (25)$$

The perturbation terms on the right hand side of (25) takes two forms, which are either phase-dependent $u_l^* u_m u_n$ ($l \neq m, n; m, n \neq 0$) or phase-independent $|u_n|^2 u_0$ ($n \neq 0$). Phase-dependent forcing terms $u_l^* u_m u_n$ ($l \neq m, n; m, n \neq 0$) yield ghost pulse generation when the bit is zero and amplitude fluctuation of u_0 when the bit slot is occupied by a signal, as a result of nonlinear interactions with nonzero bits u_l, u_m and u_n . They are commonly referred to as intra-channel

FWM. Phase-independent terms $|u_n|^2 u_0$ ($n \neq 0$) bring about a timing shift of u_0 due to interaction with another nonzero bit u_n . It should be noted that the phase-independent terms do not contribute to the ghost pulse growth or energy exchange, since they maintain energy. Also, the contribution of the phase-dependent terms to the frequency and timing shifts is negligible [26]. Note that the integers l , m and n must satisfy the phase-matching condition $l = m + n$ [21,26].

5.1 Perturbed DMNLS equation

In this section, using the multiple scale method, we develop an analytical framework to study nonlinear intra-channel interactions. The key idea behind multiple scale approach is the same as in Section 3, i.e., to introduce fast and slow scales and thus eliminate fast pulse dynamics due to large and periodically varying dispersion. The obtained equation is the DMNLS equation perturbed by interaction terms. The leading order multiple scale approximation is found to agree with the analytical model presented in [19,20]

We start the analysis with the perturbed NLS equation of the form

$$i \frac{\partial u_0}{\partial z} + \frac{D(z)}{2} \frac{\partial^2 u_0}{\partial t^2} = -g(z)|u_0|^2 u_0 - 2g(z)|u_j|^2 u_0 - g(z)u_l^* u_m u_n, \quad (26)$$

where the second and third term of the right hand side is intra-channel XPM and FWM term respectively, where $j \neq 0$ and $l = m + n$ ($m, n \neq 0$) from the phase matching condition.

We carry out the same multiple scale expansion as in Section 3. We expand the field u_k ($k = 0, l, m, n$) in powers of z_a

$$u_k(\zeta, z, t) = u_k^{(0)}(\zeta, z, t) + z_a u_k^{(1)}(\zeta, z, t) + \dots, \quad (27)$$

to find the leading order solution at $O(1/z_a)$:

$$\hat{u}_k^{(0)}(\zeta, z, \omega) = \hat{U}_k(z, \omega) \exp[-iC(\zeta)\omega^2/2] \quad (28)$$

(note $\hat{U}_k(z, \omega) = \hat{U}_0(z, \omega) \exp(-i\omega k T)$). At $O(1)$ in the expansion, we have (in the frequency domain)

$$i \frac{\partial \hat{u}_0^{(1)}}{\partial \zeta} - \frac{\Delta(\zeta)}{2} \omega^2 \hat{u}_0^{(1)} = -\hat{P}^{(1)},$$

$$\hat{P}^{(1)} = i \frac{\partial \hat{u}_0^{(0)}}{\partial z} - \frac{\langle D \rangle}{2} \omega^2 \hat{u}_0^{(0)} + g(z) \mathcal{F} \left[|u_0^{(0)}|^2 u_0^{(0)} + 2|u_j^{(0)}|^2 u_0^{(0)} + u_l^{(0)*} u_m^{(0)} u_n^{(0)} \right]. \quad (29)$$

The nonsecular condition (10) yields the following equation for \hat{U}_0 :

$$i \frac{\partial \hat{U}_0}{\partial z} - \frac{\langle D \rangle}{2} \omega^2 \hat{U}_0 = - \left\langle g(\zeta) \exp(iC\omega^2/2) \left(\mathcal{F} \left[|u_0^{(0)}|^2 u_0^{(0)} \right] + \mathcal{F} \left[2|u_j^{(0)}|^2 u_0^{(0)} \right] + \mathcal{F} \left[u_l^{(0)*} u_m^{(0)} u_n^{(0)} \right] \right) \right\rangle$$

$$\equiv -(\hat{\mathcal{I}}_{\text{SPM}} + \hat{\mathcal{I}}_{\text{XPM}} + \hat{\mathcal{I}}_{\text{FWM}}), \quad (30)$$

where

$$\begin{aligned} \hat{\mathcal{I}}_{\text{SPM}} = & \int_{-\infty}^{\infty} \int_{-\infty}^{\infty} r(\omega_1\omega_2) \hat{U}_0(z, \omega + \omega_1) \hat{U}_0(z, \omega + \omega_2) \hat{U}_0^*(z, \omega + \omega_1 + \omega_2) \\ & \times d\omega_1 d\omega_2, \end{aligned} \quad (31a)$$

$$\begin{aligned} \hat{\mathcal{I}}_{\text{XPM}} = & 2 \int_{-\infty}^{\infty} \int_{-\infty}^{\infty} r(\omega_1\omega_2) \hat{U}_0(z, \omega + \omega_1) \hat{U}_j(z, \omega + \omega_2) \hat{U}_j^*(z, \omega + \omega_1 + \omega_2) \\ & \times d\omega_1 d\omega_2, \end{aligned} \quad (31b)$$

$$\begin{aligned} \hat{\mathcal{I}}_{\text{FWM}} = & \int_{-\infty}^{\infty} \int_{-\infty}^{\infty} r(\omega_1\omega_2) \hat{U}_m(z, \omega + \omega_1) \hat{U}_n(z, \omega + \omega_2) \hat{U}_l^*(z, \omega + \omega_1 + \omega_2) \\ & \times d\omega_1 d\omega_2, \end{aligned} \quad (31c)$$

If we keep only the term $\hat{\mathcal{I}}_{\text{SPM}}$ in (30), this is reduced to the DMNLS equation obtained previously in (11).

5.2 Energy transfer

We now apply (30) to study nonlinear intra-channel interactions. Since the energy of u_0 is computed by $W_0 = (1/2\pi) \int_{-\infty}^{\infty} |\hat{U}_0(z, \omega)|^2 d\omega$ in the frequency domain, the energy change is obtained from

$$\frac{dW_0}{dz} = \frac{1}{2\pi} \int_{-\infty}^{\infty} \left(\hat{U}_0^* \frac{\partial \hat{U}_0}{\partial z} + \hat{U}_0 \frac{\partial \hat{U}_0^*}{\partial z} \right) d\omega = \frac{i}{2\pi} \int_{-\infty}^{\infty} \left(\hat{U}_0^* \hat{\mathcal{I}}_{\text{FWM}} - \hat{U}_0 \hat{\mathcal{I}}_{\text{FWM}}^* \right) d\omega. \quad (32)$$

By using (12) and (28) and employing the inverse Fourier transform, we find

$$\begin{aligned} \frac{dW_0}{dz} = & \frac{i}{(2\pi)^3} \int_0^1 d\zeta g(\zeta) \int_{-\infty}^{\infty} d\omega_1 d\omega_2 d\omega [\hat{u}_0^*(\zeta, z, \omega) \hat{u}_m(\zeta, z, \omega + \omega_1) \\ & \times \hat{u}_n(\zeta, z, \omega + \omega_2) \hat{u}_l^*(\zeta, z, \omega + \omega_1 + \omega_2) - \text{c.c.}] \\ = & \frac{i}{(2\pi)^3} \int_0^1 d\zeta g(\zeta) \int_{-\infty}^{\infty} dt_1 dt_2 dt_3 dt_4 d\omega_1 d\omega_2 d\omega \{ u_0^*(\zeta, z, t_1) u_m(\zeta, z, t_2) \\ & \times u_n(\zeta, z, t_3) u_l^*(\zeta, z, t_4) \exp[-i\omega(-t_1 + t_2 + t_3 - t_4)] \exp[-i\omega_1(t_2 - t_4)] \\ & \times \exp[-i\omega_2(t_3 - t_4)] - \text{c.c.} \} \\ = & i \int_0^1 d\zeta g(\zeta) \int_{-\infty}^{\infty} dt [u_0^*(\zeta, z, t) u_m(\zeta, z, t) u_n(\zeta, z, t) u_l^*(\zeta, z, t) - \text{c.c.}], \end{aligned} \quad (33)$$

where we used the identity $\int_{-\infty}^{\infty} d\omega \exp(i\omega t) = 2\pi\delta(t)$, and $t = t_1$. Energy change $\Delta W_0(z) = W_0(z) - W_0(0)$ is computed by integration of (33).

When $\langle D \rangle = 0$, \hat{u}_k is independent of z , so that the right-hand side of (33) is constant in terms of z , and thus ΔW_0 grows linearly with respect to distance

$$\Delta W_0(z) = \bar{Q}_{m,n} z,$$

$$\bar{Q}_{m,n} = i \int_0^1 d\zeta g(\zeta) \int_{-\infty}^{\infty} dt [u_0^*(\zeta, t) u_m(\zeta, t) u_n(\zeta, t) u_l^*(\zeta, t) - \text{c.c.}] \quad (34)$$

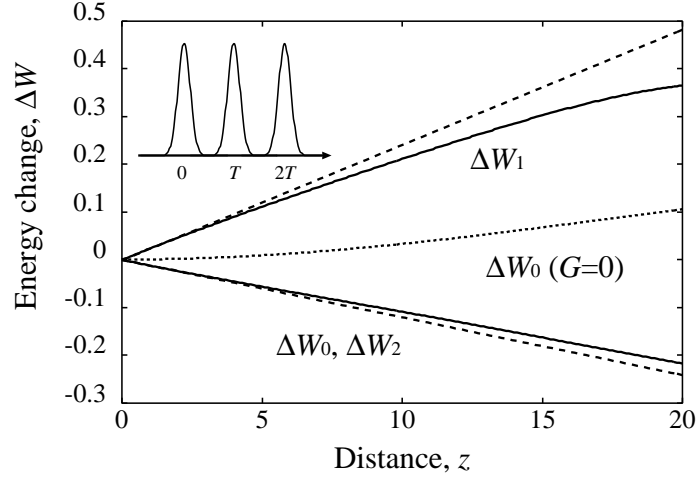


Fig. 7. Growth of energy change of the signals in a 111 bit pattern in a lossy case ($\Gamma = 10$). The solid curves are results of direct numerical simulation of Eq. (1) and the dashed curves are the results obtained from Eq. (34) with (36). The dotted curve shows the energy change ΔW_0 when $G = 0$ obtained from direct numerical simulation.

representing the growth rate. Thus we have a resonant growth situation.

So far no particular restrictions on the form of the pulse shape have been imposed in the analysis. In order to obtain explicit formulae to compute the energy exchange, in the following we assume that a signal is given by a Gaussian pulse

$$u_k(\zeta, t) = \frac{\alpha}{\sqrt{2\pi\xi(\zeta)}} \exp\left[-\frac{(t - kT)^2}{2\xi(\zeta)}\right], \quad \xi(\zeta) = \beta + iC(\zeta). \quad (35)$$

Substituting (35) to (34), we find

$$\bar{Q}_{m,n} = \frac{i\alpha^4}{4\pi^2} \sqrt{\frac{\pi}{2\beta}} \int_0^1 \left[\frac{g(\zeta)}{|\xi(\zeta)|} \exp\left(-\frac{(m^2 + n^2)\beta + 2imnC(\zeta)}{2|\xi(\zeta)|^2} T^2\right) - \text{c.c.} \right] d\zeta, \quad (36)$$

where we used the condition $l = m + n$. These formulae agree with the results obtained directly from (26) [20].

Equation (32) provides a more general result when $\langle D \rangle \neq 0$ and the pulse is pre-chirped by the cumulative dispersion C_0 . We compute W_0 by rewriting $\hat{U}(z, \omega)$ as

$$\tilde{U}(z, \omega) = \hat{U}(z, \omega) \exp[-i(C_0 + \langle D \rangle z)\omega^2/2] \quad (37)$$

and substituting to $\hat{\mathcal{T}}_{\text{FWM}}$ (31c) and dW_0/dz (32). Furthermore, when we take a limit $s \rightarrow 0$, this equation allows one to describe the evolution of energy change in a highly dispersed system [27,28] i.e., large and constant dispersion fibers.

Figure 7 shows plots of the energy change of the bits u_0 , u_1 , and u_2 for the bit pattern '111' ($k = 0, 1, 2$; see the inset) and 0 elsewhere, obtained

from Eq. (34) with (36) calculated numerically and from direct simulation of (1). The parameters that are used in the calculation are $\alpha = \sqrt{2\pi}$, $\beta = 1.0$, $T = 8.3$, $\Gamma = 10$, $z_a = 0.1$, and $s = 22$ in dimensionless units. With the choice of $t_* = 3$ ps, $\nu = 2.5 \text{ W}^{-1}\text{km}^{-1}$, $P_* = 1$ mW, i.e. $z_{\text{NL}} = 400$ km and $k_*'' (= -t_*^2/z_{\text{NL}}) = -2.25 \times 10^{-2} \text{ ps}^2/\text{km}$, they correspond to the transmission of the pulses with the path-average peak power 1 mW, the full-width at half-maximum (FWHM) $\tau_{\text{FWHM}} = 5$ ps (minimum), and the bit interval $t_{\text{bit}} = 25$ ps (corresponding to the bit rate $B = 40$ Gbit/s), in a dispersion-managed fiber with the period 40 km, $k'' = \pm 20 \text{ ps}^2/\text{km}$, and the loss 0.22 dB/km. We note that $\Delta W_2 = \Delta W_0$ and $\Delta W_1 = -2\Delta W_0$ from symmetry and the conservation of total energy. In this case, the only combination of integers satisfying the phase-matching condition is $(l, m, n) = (2, 1, 1)$. Good agreement between the analytical and the numerical results can be seen. It should be noted that over longer distance, as the energy transfer increases, other effects become important and the assumptions in the model must be modified. We also note that, in the limit of $G \rightarrow 0$ (i.e., $g(z) = 1$), we have $\bar{Q}_{m,n} \rightarrow 0$ [20]. This implies that in a lossless system the energy change is reduced substantially. This suppression is attributed to the absence of amplification, which introduces periodicity into the system and in turn brings about strong resonance. In Fig. 7 we also show the energy change of u_0 in a lossless case obtained from direct simulation. As expected, when $G \rightarrow 0$ suppression of the energy change is observed even with the same value of path-average signal power as in the lossy case, which further confirms the analysis.

5.3 Frequency and timing shifts

The frequency and timing shift of u_0 is also computed from (30). Noting that the mean frequency is given by $\Omega_0 = \int_{-\infty}^{\infty} \omega |\hat{U}_0|^2 d\omega / \int_{-\infty}^{\infty} |\hat{U}_0|^2 d\omega$, we find the frequency shift due to the XPM term to be calculated from

$$\frac{d\Omega_0}{dz} = \frac{\int_{-\infty}^{\infty} \omega \left(\hat{U}_0^* \frac{\partial \hat{U}_0}{\partial z} + \hat{U}_0 \frac{\partial \hat{U}_0^*}{\partial z} \right) d\omega}{\int_{-\infty}^{\infty} |\hat{U}_0|^2 d\omega} = \frac{\int_{-\infty}^{\infty} i\omega \left(\hat{U}_0^* \hat{\mathcal{I}}_{\text{XPM}} - \hat{U}_0 \hat{\mathcal{I}}_{\text{XPM}}^* \right) d\omega}{\int_{-\infty}^{\infty} |\hat{U}_0|^2 d\omega}. \quad (38)$$

Using (12) and (28) and employing the inverse Fourier transform, we have

$$\begin{aligned} & \int_{-\infty}^{\infty} i\omega \left(\hat{U}_0^* \hat{\mathcal{I}}_{\text{XPM}} - \hat{U}_0 \hat{\mathcal{I}}_{\text{XPM}}^* \right) d\omega \\ &= \frac{2}{(2\pi)^2} \int_0^1 d\zeta g(\zeta) \int_{-\infty}^{\infty} d\omega_1 d\omega_2 d\omega i\omega \left[\hat{u}_0^*(\zeta, z, \omega) \hat{u}_0(\zeta, z, \omega + \omega_1) \right. \\ & \quad \left. \times \hat{u}_j(\zeta, z, \omega + \omega_2) \hat{u}_j^*(\zeta, z, \omega + \omega_1 + \omega_2) - \text{c.c.} \right] \\ &= \frac{2}{(2\pi)^2} \int_0^1 d\zeta g(\zeta) \int_{-\infty}^{\infty} dt_1 dt_2 dt_3 dt_4 d\omega_1 d\omega_2 d\omega i\omega \left\{ u_0^*(\zeta, z, t_1) u_0(\zeta, z, t_2) \right. \end{aligned}$$

$$\begin{aligned}
& \times u_j(\zeta, z, t_3) u_j^*(\zeta, z, t_4) \exp[-i\omega(-t_1 + t_2 + t_3 - t_4)] \exp[-i\omega_1(t_2 - t_4)] \\
& \times \exp[-i\omega_2(t_3 - t_4)] - \text{c.c.} \} \\
= & 2 \int_0^1 d\zeta g(\zeta) \int_{-\infty}^{\infty} dt_1 dt_4 \left[u_0^*(t_1) u_0(t_4) |u_j(t_4)|^2 \int_{-\infty}^{\infty} d\omega i\omega \exp[i\omega(t_1 - t_4)] \right. \\
& \left. - u_0(t_1) u_0^*(t_4) |u_j(t_4)|^2 \int_{-\infty}^{\infty} d\omega i\omega \exp[-i\omega(t_1 - t_4)] \right] \\
= & -2(2\pi) \int_0^1 d\zeta g(\zeta) \int_{-\infty}^{\infty} dt_4 \left(\frac{\partial u_0^*}{\partial t_4} u_0(t_4) + \frac{\partial u_0}{\partial t_4} u_0^*(t_4) \right) |u_j(t_4)|^2 \\
= & -2(2\pi) \int_0^1 d\zeta g(\zeta) \int_{-\infty}^{\infty} dt \frac{\partial |u_0|^2}{\partial t} |u_j|^2 \\
= & 2(2\pi) \int_0^1 d\zeta g(\zeta) \int_{-\infty}^{\infty} dt |u_0|^2 \frac{\partial |u_j|^2}{\partial t}, \tag{39}
\end{aligned}$$

where we have used the relations $\int_{-\infty}^{\infty} d\omega \exp(i\omega t) = 2\pi\delta(t)$, $\int_{-\infty}^{\infty} dt' f(t') \int_{-\infty}^{\infty} d\omega \times i\omega \exp[\pm i\omega(t' - t)] = \mp 2\pi \int_{-\infty}^{\infty} dt' (df/dt') \delta(t' - t) = \mp 2\pi(df/dt)$, and $t = t_4$. Thus $d\Omega_0/dz$ is obtained from (38) as

$$\frac{d\Omega_0}{dz} = 2 \int_0^1 d\zeta g(\zeta) \frac{\int_{-\infty}^{\infty} |u_0(\zeta, z, t)|^2 \frac{\partial}{\partial t} |u_j(\zeta, z, t)|^2 dt}{\int_{-\infty}^{\infty} |u_0(\zeta, z, t)|^2 dt}, \tag{40}$$

where we used $\int_{-\infty}^{\infty} |\hat{U}_0(z, \omega)|^2 d\omega = \int_{-\infty}^{\infty} |\hat{u}_0(\zeta, z, \omega)|^2 d\omega = 2\pi \int_{-\infty}^{\infty} |u_0(\zeta, z, t)|^2 dt$. Note that, when $\langle D \rangle = 0$, \hat{u}_k is independent of z , so that the right-hand side of (40) is constant in terms of z .

The frequency shift yields the shift of the central temporal position of the pulse $t_0 = \int_{-\infty}^{\infty} t |u_0|^2 dt / W_0$ through GVD:

$$\frac{dt_0}{dz} = D(z) \Omega_0(z). \tag{41}$$

The timing shift $\Delta t_0(z) = t_0(z) - t_0(0)$ is obtained by integration of (40) with $\Omega_0(0) = 0$ and using (41). Interchanging the order of integration yields

$$\begin{aligned}
\Delta t_0(z) &= \int_0^z D(z') \left[\int_0^{z'} \frac{d\Omega_0}{dz''} dz'' \right] dz' = \int_0^z \frac{d\Omega_0}{dz''} \left[\int_{z''}^z D(z') dz' \right] dz'' \\
&= \int_0^z \frac{d\Omega_0}{dz''} (\bar{D}(z) - \bar{D}(z'')) dz'' = \delta t_0^{(1)}(z) + \delta t_0^{(2)}(z), \tag{42}
\end{aligned}$$

where

$$\delta t_0^{(1)}(z) = \bar{D}(z) \Omega_0(z), \tag{43}$$

$$\delta t_0^{(2)}(z) = \int_0^z \left(-\frac{d\Omega_0}{dz''} \right) \bar{D}(z'') dz''. \tag{44}$$

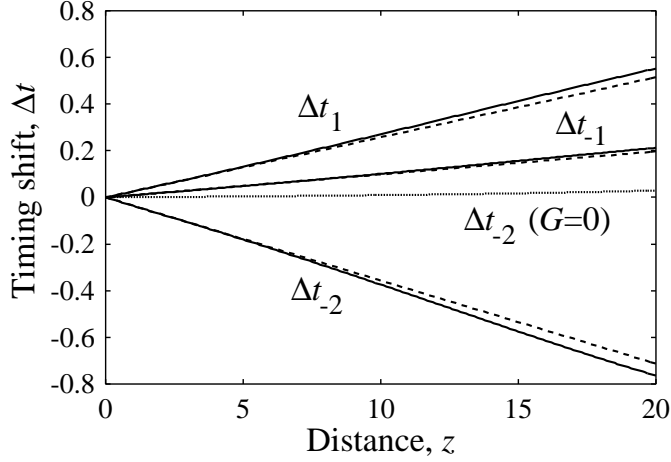


Fig. 8. Growth of timing shifts of the signals centered at $t = -2T$ (Δt_{-2}), $t = -T$ (Δt_{-1}) and $t = T$ (Δt_1) in a 1101 bit pattern in a lossy case ($\Gamma = 10$). The solid curves are results of direct numerical simulation of Eq. (1) and the dashed curves are the results obtained from Eq. (45). The dotted curve shows the timing shift Δt_{-2} when $G = 0$ obtained from direct numerical simulation.

Thus the timing shift is composed of two terms: $\delta t_0^{(1)}$ and $\delta t_0^{(2)}$. We note that when $\bar{D}(z) = 0$, the timing shift is given by $\delta t_0^{(2)}$ alone in (42). In the case of zero average dispersion, this condition corresponds to $C(z) = 0$, namely at chirp-free points.

When $\langle D \rangle = 0$, $d\Omega_0/dz$ is constant in terms of z and $\bar{D}(z) = C(\zeta)$, from (42) and (44) the timing shift $\delta t_0^{(2)}$ grows linearly with respect to distance

$$\delta t_0^{(2)}(z) = \bar{P}_n z, \quad (45)$$

$$\bar{P}_n = -2 \int_0^1 d\zeta C(\zeta) g(\zeta) \frac{\int_{-\infty}^{\infty} |u_0(\zeta, t)|^2 \frac{\partial}{\partial t} |u_j(\zeta, t)|^2 dt}{\int_{-\infty}^{\infty} |u_0(\zeta, t)|^2 dt}.$$

In the following, we assume a signal given by a Gaussian pulse (35). Substituting (35) to (45), we have

$$\bar{P}_n = -\frac{\alpha^2 \beta n T}{\sqrt{2\pi}} \int_0^1 \frac{C(\zeta) g(\zeta)}{|\xi(\zeta)|^3} \exp\left(-\frac{\beta n^2 T^2}{2|\xi(\zeta)|^2}\right) d\zeta. \quad (46)$$

These formulae agree with the results obtained directly from (26) [19].

Figure 8 shows plots of the timing shift of the bits u_{-2} , u_{-1} , and u_1 for the bit pattern ‘1101’ ($k = -2, -1, 0, 1$), obtained from Eq. (45) with (46) calculated numerically and from direct simulation of (1). In order to compute

the timing shift of u_k , $k \neq 0$ using (45), we need to shift the bit pattern by $-kT$ so that the central position of u_k is moved to $t = 0$, and relabel all the bit slots correspondingly. Δt_{-2} , for instance, is given by $\Delta t_0(n = 1) + \Delta t_0(n = 3)$. Once again good agreement between the analytical and the numerical results can be seen. It should be noted that, in the limit of $G \rightarrow 0$ (i.e., $g(z) = 1$), we have $\bar{P}_n \rightarrow 0$ [19]. This implies substantial reduction of timing shifts, like energy change. We also show in Fig. 8 the timing shift of u_{-2} in a lossless case obtained from direct simulation. As predicted, a significant suppression of the timing shift is observed even with the same value of path-average power as in the lossy case.

6 Conclusion

An analytical model has been developed which clarifies fundamental properties of quasi-linear dispersion-managed transmission. Quasi-linear pulses can be viewed as degenerate limit of a DM soliton. It was found that dispersion management mitigates nonlinearity by $O(\log s/s)$ in quasi-linear regime. The periodic perturbation due to loss and lumped amplification modifies the averaged dynamics of quasi-linear transmission depending on the relative position of the lumped amplifiers. The amount of spectral reshaping and the nonlinear chirp in the frequency domain due to residual nonlinearity was quantified. Periodic dispersion management results in a resonant intra-channel pulse interactions because of periodic forcing due to lumped amplification supported by phase matching in the time domain. The DMNLS equation obtained from the perturbed NLS equation by means of a multiple scale approach was found to provide a unified analytical framework to study long-scale dynamics of the propagation and interaction of quasi-linear pulses and DM solitons.

Acknowledgments

The authors would like to acknowledge Gino Biondini and Andrew Docherty for providing us with useful remarks. This work was partially supported by NSF grants ECS-9800152, DMS-0070792.

References

1. J. P. Gordon and H. A. Haus, "Random walk of coherently amplified solitons in optical fiber transmission," *Opt. Lett.* **11**, 665 (1986).
2. M. Suzuki, I. Morita, N. Edagawa, S. Yamamoto, H. Taga, and S. Akiba, "Reduction of Gordon-Haus timing jitter by periodic dispersion compensation in soliton transmission," *Electron. Lett.* **31**, 2027 (1995).
3. N. J. Smith, F. M. Knox, N. J. Doran, K. J. Blow, and I. Bennion, "Enhanced power solitons in optical fibres with periodic dispersion management," *Electron. Lett.* **32**, 54 (1996).
4. M. J. Ablowitz, T. Hirooka, and G. Biondini, "Quasi-linear optical pulses in strongly dispersion-managed transmission systems," *Opt. Lett.* **26**, 459 (2001).

5. M. J. Ablowitz and T. Hirooka, 'Managing nonlinearity in strongly dispersion-managed optical pulse transmission,' *J. Opt. Soc. Am. B* **11**, 425 (2002).
6. C. Kurtzke, 'Suppression of fiber nonlinearities by appropriate dispersion management,' *IEEE Photon. Technol. Lett.* **5**, 1250 (1993).
7. R. W. Tkach, A. R. Chraplyvy, F. Forghieri, A. H. Gnauck, and R. M. Derosier, 'Four-photon mixing and high-speed WDM systems,' *IEEE J. Lightwave Technol.* **13**, 841 (1995).
8. N. S. Bergano, C. R. Davidson, M. Ma, A. Pillipetskii, S. G. Evangelides, H. D. Kidorf, J. M. Darcie, E. Golovchenko, K. Rottwitt, P. C. Corbett, R. Menges, M. A. Mills, B. Pedersen, D. Peckham, A. A. Abramov, and A. M. Vengsarkar, in *Digest of Optical Fiber Communication Conference* (Optical Society of America, Washington, D.C., 1998), postdeadline paper PD12.
9. R. Horne, "Collision induced timing jitter and four-wave mixing in wavelength division multiplexing soliton systems," Ph. D dissertation, Department of Applied Mathematics, University of Colorado at Boulder (2001).
10. M. J. Ablowitz and G. Biondini, "Multiscale pulse dynamics in communication systems with dispersion management," *Opt. Lett.* **23**, 1668 (1998).
11. R. J. Essiambre, B. Mikkelsen, and G. Raybon, 'Intra-channel cross-phase modulation and four-wave mixing in high-speed TDM systems,' *Electron. Lett.* **35**, 1576 (1999).
12. P. V. Mamyshev and N. A. Mamysheva, "Pulse-overlapped dispersion-managed data transmission and intrachannel four-wave mixing," *Opt. Lett.* **24**, 1454 (1999).
13. H. Sugahara, H. Kato, and Y. Kodama, "Maximum reductions of collision induced frequency shift in soliton-WDM systems with dispersion compensation," *Electron. Lett.* **33**, 1065 (1997).
14. T. Hirooka and A. Hasegawa, "Chirped soliton interaction in strongly dispersion-managed wavelength-division-multiplexing systems," *Opt. Lett.* **23**, 768 (1998).
15. P. V. Mamyshev and L. F. Mollenauer, "Soliton collisions in wavelength-division-multiplexed dispersion-managed systems," *Opt. Lett.* **24**, 448 (1999).
16. M. J. Ablowitz, G. Biondini, and E. S. Olson, "Incomplete collisions of wavelength-division-multiplexed dispersion-managed solitons," *J. Opt. Soc. Am. B* **18**, 577 (2001).
17. J. Martensson, A. Berntson, M. Westlund, A. Danielsson, P. Johannisson, D. Anderson, and M. Lisak, 'Timing jitter owing to intrachannel pulse interactions in dispersion-managed transmission systems,' *Opt. Lett.* **26**, 55 (2001).
18. S. Kumar, 'Intrachannel four-wave mixing in dispersion managed RZ systems,' *IEEE Photon. Technol. Lett.* **13**, 800 (2001).
19. M. J. Ablowitz and T. Hirooka, "Intra-channel pulse interactions in dispersion-managed transmission systems: timing shifts," *Opt. Lett.* **26**, 1846 (2001).
20. M. J. Ablowitz and T. Hirooka, "Intra-channel pulse interactions in dispersion-managed transmission systems: energy transfer," *Opt. Lett.* **27**, 203 (2002).
21. M. J. Ablowitz and T. Hirooka, "Resonant nonlinear intra-channel interactions in strongly dispersion-managed transmission systems" *Opt. Lett.* **25**, 1750 (2000).
22. M. J. Ablowitz, G. Biondini, and E. Olson, "On the evolution and interaction of dispersion-managed solitons," in *Massive WDM and TDM Soliton Transmission Systems*, Ed. A. Hasegawa (Kluwer, Dordrecht, 2000).
23. S. Shen, C. -C. Chang, H. P. Sardesai, V. Binjrajka, and A. M. Weiner, 'Effects of self-phase modulation on sub-500 fs pulse transmission over dispersion compensated fiber links,' *J. Lightwave Technol.* **17**, 452 (1999).

24. S. T. Cundiff, B. C. Collings, L. Boivin, M. C. Nuss, K. Bergman, W. H. Knox, and S. G. Evangelides, Jr., 'Propagation of highly chirped pulses in fiber-optic communications systems,' *J. Lightwave Technol.* **17**, 811 (1999).
25. R. -M. Mu, T. Yu, V. S. Grigoryan, and C. R. Menyuk, 'Convergence of the CRZ and DMS formats in WDM systems using dispersion management,' in *Digest of Optical Fiber Communication Conference* (Optical Society of America, Washington, D.C., 2000), paper FC1.
26. M. J. Ablowitz and T. Hirooka, "Resonant intra-channel pulse interactions in dispersion-managed transmission systems," submitted to *IEEE J. Sel. Topics Quantum Electron.* (2002).
27. A. Mecozzi, C. B. Claussen, and M. Shtaif, 'Analysis of intrachannel nonlinear effects in highly dispersed optical pulse transmission,' *IEEE Photon. Technol. Lett.* **12**, 392 (2000).
28. A. Mecozzi, C. B. Claussen, and M. Shtaif, 'System impact on intra-channel nonlinear effects in highly dispersed optical pulse transmission,' *IEEE Photon. Technol. Lett.* **12**, 1633 (2000).